Renewable Energy 177 (2021) 1438–1450

Contents lists available at ScienceDirect

Renewable Energy

journal homepage: www.elsevier.com/locate/renene

Coordinated operation of water and electricity distribution networks with variable renewable energy and distribution locational marginal pricing☆

Lawryn Edmonds [a, *], Melanie Derby [b], Mary Hill [c], Hongyu Wu [a]

[a] Mike Wiegers Department of Electrical and Computer Engineering, Kansas State University, Manhattan, KS, United States
[b] Alan Levin Department of Mechanical and Nuclear Engineering, Kansas State University, Manhattan, KS, United States
[c] Department of Geology, University of Kansas, Lawrence, KS, United States

ARTICLE INFO

Article history:
Received 4 March 2021
Received in revised form
6 May 2021
Accepted 29 May 2021
Available online 11 June 2021

Keywords:
Water-energy nexus
Distribution locational marginal price
Uncertainty
Probability efficient point

ABSTRACT

Water and electricity distribution networks are two highly interdependent and critical infrastructures in the world today. This paper investigates the coupling of water and electricity distribution networks through the electrical energy demand of water pumps. Further, with additional variable renewable energy (VRE) sources in the distribution system, utilities face significant challenges stemming from the VRE stochasticity. In this paper, a coordinated operational model of urban water and electricity distribution networks is proposed. Stochastic VRE generation is handled by using a data-driven probability efficient point (PEP) method based on historical wind and solar datasets without the need for any probability distribution function. Case studies are performed on a modified Institute of Electrical and Electronics Engineers (IEEE) 13-node electricity distribution network coupled with a 10-node water distribution network, typical of a small-town setting. Results show the impact of coordinating water and energy networks on the cost of operation and the distribution locational marginal prices (DLMPs). The inclusion of water tanks as alternative storage devices in the electricity distribution network are shown to slightly reduce voltage violations, line congestion, and VRE curtailments in a case with high VRE penetration.

1. Introduction

Water and electricity networks are two critical infrastructures in today's society. Though typically operated independently, these infrastructures are profoundly interdependent. For example, in 2015, 41% of the water withdrawn in the U.S. was sent to electrical power plants mainly for cooling purposes, with 3% of this water being consumed [1]. On the other hand, water pumps require electrical energy to pump water to water treatment centers and for use in the agriculture industry [2]. The agriculture sector is responsible for 43% of the total water withdrawn in North America [3]. Further, about 80% of municipal water costs are for electricity, and municipal water networks consume around 3–4% of U.S. energy and as much as 13% when including residential water energy usage [4]. Anticipated increases in water scarcity, variability, and uncertainty within the water network, particularly during extreme events, can lead to vulnerabilities in the U.S. energy network [2].

Synergies between water and electricity networks have long been studied by researchers and governmental entities alike. For example, authors in Refs. [5,6] present long-term integrated planning problems for water and electricity systems in the New England region in the U.S. and China, respectively. On the other hand, optimal operation of combined water and energy networks are considered in many works, such as [7,8]. Various other published articles define and study the water-energy nexus, dating back to the 1990s [9].

Changes over recent years have caused water and electricity utilities to improve efficiencies through cooperation. With the rise in water demands [10] and prices, as water prices in the U.S. increased nearly 40% from 2008 to 2016 [11], water utilities are forced to look at ways to reduce their operational costs and electricity usage. Additionally, variable renewable energy (VRE) sources, such as wind and photovoltaics (PVs), have increased in urban electrical distribution networks. Such changes produce significant challenges when matching the generation to the load, for instance, CAISO's “duck curve” [12].

☆ This work was supported by the National Science Foundation Grant 1856084 for the FEWtures project.

* Corresponding author.
E-mail address: lawryn@ksu.edu (L. Edmonds).

https://doi.org/10.1016/j.renene.2021.05.168
0960-1481/

Abbreviation list

ADMM	alternating direction method of multipliers
CAISO	California independent system operator
CCO	chance-constrained optimization
DER	distributed energy resource
DG	distributed generator
DLMP	distribution locational marginal price
DSO	distribution system operator
IEEE	Institute of Electrical and Electronics Engineers
IO	interval optimization
LMP	locational marginal price
MILP	mixed-integer linear programming
MINLP	mixed-integer nonlinear programming
MIQCP	mixed-integer quadratically constrained programming
PDF	probability distribution function
PEP	probability efficient point
PV	photovoltaic
RO	robust optimization
SO	stochastic optimization
SOC	second-order cone
VRE	variable renewable energy
VSP	variable speed pump
WWSIS	Western Wind and Solar Integration Study

Nomenclature

$\hat{\bullet}, \breve{\bullet}, \bar{\bullet}, \underline{\bullet}, \tilde{\bullet}, \hat{\bullet}, \breve{\bullet}$	Indicates injection, extraction, upper, lower limit, stochastic, gain, loss
$\mathbb{x}, \mathbb{y}$	ON/OFF indicator for pumps, valves
$\mathcal{T}, \mathcal{N}, \mathcal{J}, \mathcal{P}, R$	Number of timeslots, power buses/lines, water junctions, pipes, VRE sites
$\mathcal{U}, \mathcal{V}, \mathcal{K}, \mathcal{R}$	Set of water pipes with pumps, valves, junctions with tanks, reservoirs
$\Omega, \lambda, \mu, \rho$	DLMP, shadow price of energy, voltage, congestion
$A, \mathscr{F}, (a, b, c)$	Tank area, pipe characteristic, pump characteristic
$C_e, c, \xi, s, \kappa, \sigma$	Objective function, bid, value of lost load, curtailment, reactive to real power ratio, load shed
E, L, V, C	Energy, loss, voltage, congestion superscripts
ε, S	Voltage bound, apparent power flow
ρ_w, g, η, C_w	Water density, gravity, pump efficiency, pump electricity cost
f, d, h, u, ω	Water flow, demand, junction head, tank volume, pump speed ratio
G, D, B, R, P, Q, N, U	Generation, demand, battery, renewable, real, reactive, non-pump, pump superscripts
i, j, t, w	Index of node, water/electricity link, time, and segment
M, m	Large, small constant number
P, Q, L^P, L^Q	Real, reactive power flow, real, reactive losses
p, q, v	Real, reactive power injection, voltage
$r, x, \mathcal{M}$	Power line resistance, reactance, matrix
$tri, \mathbb{T}, (\mathscr{A}, \mathscr{B}, \mathscr{C})$	Triangle segment, triangle indicator, linear pump power characteristics
$u(\bullet), d\{\bullet\}, B$	Immediate upstream electricity node, downstream subtree, incidence matrix of water network
μ, l, m, W	Pipe Darcy friction factor, length, diameter, area
$\mathbb{v}, \mathbb{d}, \mathbb{p}, \zeta, \beta, \mathbb{s}, \mathbb{S}$	PEP vector data, scenario probability, selector, probability level, sample, set

Solutions commonly addressed in the literature for mismatches in power generation and load are demand response techniques and the use of energy storage resources [13]. Storage options include battery storage, concentrating solar power combined with thermal energy storage [14], and utility-scale pumped storage hydro [15,16]. These storage projects can have substantial capital costs [17]; therefore, cheaper energy storage ideas are needed. A less costly avenue for energy storage could be through gravitational potential energy storage in existing water tanks.

We aim to address these challenges by providing a framework for urban water and energy networks to cooperate by reducing peak electricity loads and VRE curtailments through flexibility in the water pump power consumption. For example, electric utility operators can shift pump demand by using water tanks as storage devices. The water network subsequently provides a service to the electricity network and must be rewarded as such.

One way to accurately reward active resources in the distribution system is by buying and selling energy at the true cost of electricity at a node, namely, the distribution locational marginal price (DLMP). The DLMP is the marginal cost to serve the next unit of power at a distribution network node. It is similar to the locational marginal price (LMP) of the transmission network. The DLMP mechanism embedded into future distribution energy markets is a useful tool in integrating various types of distributed energy resources (DERs) into the existing electricity distribution network by incentivizing ancillary services. Further, DLMPs indicate the health of the network as they are higher when the distribution system sees operational issues, e.g., congestion on lines and voltage violations at nodes. This DLMP increase is due to a cost-causation pricing mechanism to the node that provokes these operational issues. The DLMP mechanism itself serves as a financial incentive.

Several methods for day-ahead scheduling of water pumps based on electricity prices have been proposed in the literature [18–24]. Works [18–21,23], and [24] consider drinking water pumps, while [22] considers both freshwater and wastewater pumps in their model. Further, authors in Ref. [18] propose a mixed-integer second-order cone program to solve the water supply network using a fixed price scheme. Alternating direction method of multipliers (ADMM) is used to provide suboptimal solutions to the water network's biconvex objective function that minimizes the cost of electricity used to power the pumps. An electricity network and the corresponding constraints are not considered. A second pump scheduling method considers a coupled water and electricity network with physical constraints for both in Ref. [19]. The result is a nonconvex, quadratically-constrained quadratic problem using feasible point pursuit-successive convex approximation methods to solve. Then, a distributed ADMM-based algorithm is used to update water and energy variables in an alternating fashion. Outputs from DERs and electricity prices are considered as fixed values. These approaches are not suitable to the present problem because a coupled model must be considered to capture the impacts one network has on the other. Also, it is important to consider the variability of renewable resources because their forecasts do not always match their actual power output. Finally, fixed energy prices do not reflect the impact actions in the water network have on the price of electricity.

Two recently published papers [20,21] are most relevant to this work. First, Oikonomou et al. using a mixed-integer linear programming (MILP) model, consider optimizing water pump and tank schedules with respect to a fixed electricity price while maximizing

the profit to the water network for providing services, such as demand response and frequency regulation, to the electricity transmission network [20]. A sensitivity analysis of the number of tanks in a water distribution network was also pursued in this work. Then, Oikonomou and Parvania provided an MILP model of the coupled water and transmission network and constraints in Ref. [21], where the impact on the LMP was further investigated. A case where the transmission system operator optimizes water network flexibility was considered. However, water valves, VRE units, and stochasticity in the model are not considered.

In contrast to the transmission system, the electricity distribution network is characterized by a lower x/r ratio and a radial topology. Smaller than their transmission counterparts, peak loads of typical distribution network feeders range from 0.6 to 28.5 MW, and typical lengths range from 1.1 to 32.6 miles [36]. Further, DERs, voltage limits, power losses, etc., are prominent in the electricity distribution network and need to be taken into account. Therefore, Oikonomou and Parvania, in Ref. [22] also considered a coupled water and energy distribution-level model, where fixed hourly price tariffs are applied to the water network. In this mixed-integer quadratically constrained programming (MIQCP) model, the water treatment facility is also treated as a flexible load. Again, stochasticity and valves are not considered in this model. In a similar paper that considers the optimal operation of water-energy microgrids, Moazeni and Khazaei develop an MILP model that is compared against a mixed-integer nonlinear programming (MINLP) model in Ref. [23]. Although this work includes DERs and bidding in a distribution network, stochasticity of the VRE units and valves are ignored. However, Wang et al. in Ref. [24], propose a robust operation of the water-energy nexus where uncertainties in wind generation outputs are considered. The authors consider a transmission-level multi-energy system.

There has been little work in the literature on combined water and electricity distribution networks that consider VRE uncertainty to the best of the authors' knowledge. Furthermore, the impact of the coordination of the water network on the DLMP is still unknown. In this paper, we try to fill this gap by studying the optimal operation of interdependent electricity and water distribution networks under VRE uncertainty.

First, we propose an MILP model of merged power and water networks to optimally schedule pumping, tank storage, and DERs, considering both electricity and water network constraints. The pumping schedules are coupled with electricity utility demands and therefore serve as a flexible load. The water pumps respond to the price of electricity and available VRE generation and can run at higher capacities than what is necessary for the current water demand. The additional pumped water is stored in tanks for later use and, in turn, reduces electricity costs and VRE curtailment. In general, VRE generation curtailment occurs when there is insufficient ramping down capability in thermal units or when there is congestion on power lines, inhibiting the use of available wind and solar energy [25]. Since the proposed electricity distribution model does not incorporate thermal units with ramping limits, VRE units are curtailed to avoid congested lines. We optimize this model from the perspective of the electricity distribution system operator (DSO) while considering physical constraints of both networks. A significant operational cost to the water utility is the cost of supplying power to pumps. If the cost of supplying electricity is minimized, electricity costs to the water utility can also be reduced.

Second, there are multiple noteworthy optimization methods in the literature that deal with VRE uncertainty, such as chance-constrained optimization (CCO) [26], robust optimization (RO) [27], interval optimization (IO) [28], and stochastic optimization (SO) [29]. A recent review can be found in Ref. [30]. Here, we model the stochastic generation of VREs as a chance-constrained model, in which the minimum amount of VRE generation at a certain confidence level is obtained. To fully leverage a large amount of historical VRE datasets without assuming an explicit probability distribution, we adopt a data-driven probability efficient point (PEP) method to solve the chance-constrained model. The PEP, also referred to as the þ-efficient point or pLEP, was introduced by Prékopa in the 1990s [31]. This method requires no knowledge of the underlying probability distribution function (PDF) of the uncertainty - it depends only on historical VRE data. The PEP method has been successfully and extensively used to solve chance-constrained stochastic programming problems in many areas of study, such as stock market portfolio selection [32], fiber optic production planning [33], and disaster evacuation modeling [34]. A similar method to deal with uncertainty while not assuming a single PDF is described in [35], where a unit commitment model is optimized based on multiple PDFs, which has been shown to be distributionally robust.

Case studies are performed on a modified Institute of Electrical and Electronics Engineers (IEEE) 13-node electricity distribution network coupled with a 10-node water distribution network. An investigation into the capability of water tanks to serve as storage devices of excess renewable energy under the future case of a distribution market, as summarized in Ref. [37], is undergone. A key focus of future distribution markets is centered around supplying energy using marginal operating or social welfare costs. Therefore, the impact of the water network on the DLMP is investigated. The main contributions of this paper include:

(1) We propose an MILP model of coordinated water and electricity distribution networks by using a combined convex relaxation and 2D piece-wise linearization techniques while considering VRE stochasticity and DLMP in the model.
(2) Stochastic VRE generation is considered using a data-driven PEP method which optimally calculates probability efficient points utilizing historical VRE generation data without assuming any probability distribution of the data. This method allows for efficient management of uncertainty in VRE generation in the coordinated water and electricity distribution model.
(3) The effect of the water and electricity network coordination in a future distribution market considering DLMPs is shown. An exploration into the capability of reducing voltage violations and line congestion in the electricity distribution network is conducted.

Table 1 compares recently published work in this area to the contributions of this paper. Novel to this area of study, we provide an integrated MILP water and electricity distribution model that handles uncertainty of VRE resources using the PEP method. We also consider valves in our water model. More importantly, we include a study of how actions in the water network impact the DLMP and the physical condition of the electricity network.

The remainder of this paper is organized as follows. We outline the mathematical model for the linearized electricity and water networks in Section 2 and 3, respectively. Case studies utilizing water tanks as storage devices and their impact on the DLMP are provided in Section 4. We provide important observations and conclude the work in Section 5.

2. Electricity distribution model

We consider a balanced electricity distribution network, which we model using modified DistFlow equations with losses. We index the root node as 0 and order the rest of the nodes from 1 to $\mathcal{N}$, where $\mathcal{N}$ is the total number of nodes/lines. As shown in Fig. 1, line i

Table 1
Reference contribution summary.

Reference	Merged Water-Energy Network	VRE Uncertainty	Distribution Network	VRE	DLMP
Fooladivanda et al. [18]					
Zamzam et al. [19]	✓		✓	✓	
Oikonomou et al. [20,21]		✓			
Oikonomou and Parvania [22]	✓		✓		
Moazeni and Khazaei [23]	✓		✓	✓	
Wang et al. [24]	✓	✓(RO)		✓	
This work	✓	✓(PEP)	✓	✓	✓

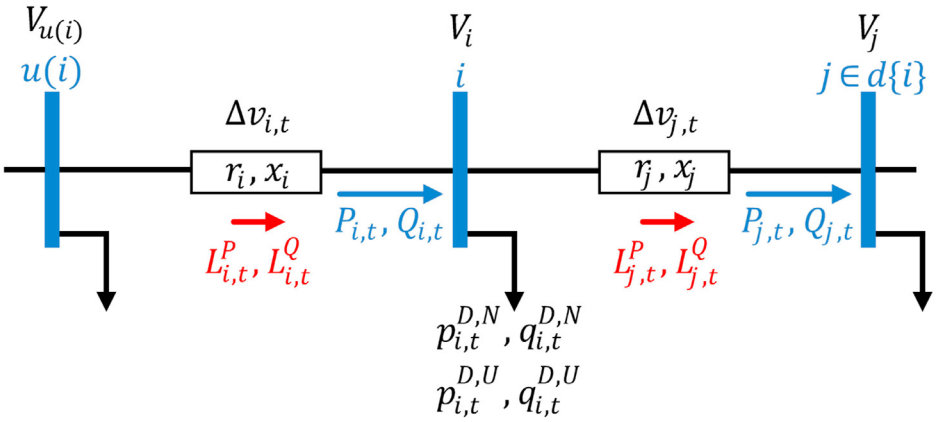

Fig. 1. Distribution branch with line i connecting bus $u(i)$ to node i. The total electrical load is comprised of non-pump ($p^{D,N}_{i,t}$) and pump ($p^{D,U}_{i,t}$) demands.

is the line connecting the upstream node, $u(i)$, and the set of downstream nodes, $d\{i\}$, to node i. All quantities related to line i are subscripted by index i, for time $t \in \mathcal{T}$. Though not pursued in this work, this model, including the DLMP decomposition, can easily be extended to a three-phase unbalanced system, as we have done in previous work, Edmonds et al. [38].

2.1. Objective function

Our objective function is defined in (1), where C_e is the least cost sum of operating the electrical distribution system.

$$C_e = \lambda^{p_0}_t \cdot p_{0,t} + \lambda^{q_0}_t \cdot q_{0,t} + \sum_{i,w,t} c^{G,P}_{i,w,t} \cdot p^G_{i,w,t} + \sum_{i,w,t} c^{G,Q}_{i,w,t} \cdot q^G_{i,w,t} + \sum_{i,t} \hat{c}^{B,P}_{i,t} \cdot \hat{p}^B_{i,t} - \sum_{i,t} \check{c}^{B,P}_{i,t} \cdot \check{p}^B_{i,t} + \sum_{i,t} \xi \cdot s^D_{i,t} \quad (1)$$

Here, $\lambda^{p_0}_t$, $\lambda^{q_0}_t$ are the real and reactive LMP prices at the substation node connected to the transmission system, and $p_{0,t}$, $q_{0,t}$ are the real and reactive net power injections at the substation node, which is assumed to be an infinite source. If these net power injections are negative, the DSO buys real or reactive power from the distribution system at the respective LMP of the substation node. Distributed generators (DGs) bid at a cost of $c^{G,p}_{i,w,t}$ for real power and $c^{G,q}_{i,w,t}$ for reactive power, where subscript w indicates the segment energy and bid block using a piecewise bidding method to approximate the fuel cost of the DGs. Variables $p^G_{i,w,t}$ and $q^G_{i,w,t}$ indicate the real and reactive segment power the generators supply. These values must lie within their respective segment constraints and sum to their total output $p^G_{i,t}$ and $q^G_{i,t}$. The reactive power output of the DG must lie within a fraction, κ^G, of the real power output. The battery energy storage system (BESS) units bid at a cost of $\hat{c}^{B,p}_{i,t}$ for extraction of power from the battery and $\check{c}^{B,p}_{i,t}$ for injection of power into the battery, where $\hat{c}^{B,p}_{i,t} \geq \check{c}^{B,p}_{i,t}$ to create a positive revenue. Variables $\hat{p}^B_{i,t}$ and $\check{p}^B_{i,t}$ indicate the power the BESS unit consumes or supplies, respectively. The final term in (1) indicates the value of lost load, ξ, and the sum of the real power demand curtailment, $s^D_{i,t}$, to penalize any load not served.

2.2. Power balance

The total system real and reactive power balance is modeled in (2)-(3), where $L^P_{i,t}$ and $L^Q_{i,t}$ are the linearized real and reactive power losses. The real and reactive power net node injection ($p_{i,t}$, $q_{i,t}$) is modeled in (4)-(5), where $p^D_{i,t}$ and $q^D_{i,t}$ are the real and reactive system power demands and $\tilde{p}^R_{i,t}$ and $\tilde{q}^R_{i,t}$ are the real and reactive stochastic VRE unit outputs.

$$p_{0,t} + \sum_i (p_{i,t} + L^P_{i,t}) = 0 \quad (2)$$

$$q_{0,t} + \sum_i (q_{i,t} + L^Q_{i,t}) = 0 \quad (3)$$

$$p_{i,t} = p^D_{i,t} - p^G_{i,t} - p^B_{i,t} - \tilde{p}^R_{i,t} \quad (4)$$

$$q_{i,t} = q^D_{i,t} - q^G_{i,t} - q^B_{i,t} - \tilde{q}^R_{i,t} \quad (5)$$

$$p^D_{i,t} = \bar{p}^D_{i,t} - s^D_{i,t} \quad (6)$$

$$0 \leq s^D_{i,t} \leq \sigma^D \cdot \bar{p}^D_{i,t} \quad (7)$$

$$p^B_{i,t} = \hat{p}^B_{i,t} - \check{p}^B_{i,t} \tag{8}$$

$$\tilde{p}^R_{i,t} = \bar{\tilde{p}}^R_{i,t} - s^R_{i,t} \tag{9}$$

$$0 \le s^R_{i,t} \le \bar{\tilde{p}}^R_{i,t} \tag{10}$$

Equation (6) determines the allocated real demand, $p^D_{i,t}$, from the requested demand, $\bar{p}^D_{i,t}$. If any, the difference between these values is captured in $s^D_{i,t}$ and is penalized in the objective function as lost load. Equation (7) limits the positive load shedding value to a fraction, σ^D, of the requested demand. Similarly, the reactive dispatched load is held to κ^D of the real dispatched load to maintain a constant load power factor.

Equation (8) defines the net real power extraction of the BESS, $p^B_{i,t}$, which is the difference between the extraction ($\hat{p}^B_{i,t}$) and injection ($\check{p}^B_{i,t}$) power. The reactive power of the battery, $q^B_{i,t}$, must lie within zero and κ^B of the real power BESS extraction. Additional BESS constraints defining the state of charge, dis/charging rates, and the minimum number of dis/charging hours can be found in our previous work [39].

Equation (9) determines the dispatched real VRE generation, $\tilde{p}^R_{i,t}$, from the expected stochastic generation, $\bar{\tilde{p}}^R_{i,t}$. (The result of the PEP method in Section 2.4.) The difference is captured in $s^R_{i,t}$. Equation (10) limits the positive curtailment value to less than the expected generation. Reactive VRE generation is held within $\pm\ \kappa^R$ of the dispatched real VRE generation.

2.3. Distribution power flow

The real and reactive power flow ($P_{i,t}$, $Q_{i,t}$) is defined in (11) and (12), and voltage, $v_{i,t}$, is defined in (13) in reference to the substation voltage $v_{0,t}$. Here, $\mathcal{M}^P_{i,j}$, $\mathcal{M}^Q_{i,j}$ are comprised of upstream and downstream incidence matrices and line resistance and reactance diagonal matrices [40]. The real and reactive power losses ($L^P_{i,t}$, $L^Q_{i,t}$) which are originally quadratic relations of the real and reactive power flow, line impedance, and nodal voltage, are approximated using a first-order Taylor series approximation around a feasible point that is obtained exogenously [41]. More detail on the approximated loss is presented in our previous work [40]. Equations (14) and (15) enforce voltage and line limit bounds, respectively. Here, ε is some small value, typically 5%, and $\bar{S}_i$ is the maximum allowable MVA line limit. Equation (15) is a linear approximation of the initially convex quadratic apparent power flow limit, $|P_{i,t}|^2 + |Q_{i,t}|^2 \le \bar{S}_i^2$. This equation models the outer approximation of the network power flow and was obtained from *Convex Optimization of Power Systems* [42].

$$P_{i,t} = p_{i,t} + \sum_{k \in d\{i\}} (p_{k,t} + L^P_{k,t}) \tag{11}$$

$$Q_{i,t} = q_{i,t} + \sum_{k \in d\{i\}} (q_{k,t} + L^Q_{k,t}) \tag{12}$$

$$v_{i,t} = v_{0,t} - \sum_{k \in \mathcal{N}} \mathcal{M}^P_{i,k} \cdot (p_{k,t} + L^P_{k,t}) - \sum_{k \in \mathcal{N}} \mathcal{M}^Q_{i,k} \cdot (q_{k,t} + L^Q_{k,t}) \tag{13}$$

$$1 - \varepsilon \le v_{i,t} \le 1 + \varepsilon \tag{14}$$

$$|P_{i,t}| + |Q_{i,t}| \le \sqrt{2} \cdot \bar{S}_i \tag{15}$$

Therefore, the DSO's optimization problem formulated in (1)-(15) integrates a real and reactive, balanced distribution system model to account for DGs, VRE units, RLs, and BESSs. This approach is unique, as indicated in Table 1. The accuracy of the electricity distribution model measurements was validated in our previous work using commercially available electricity model software, MATPOWER, and can be investigated in Ref. [40].

2.4. Data-driven probability efficient point (PEP) method

We consider the use of the PEP method to address stochastic VRE generation in the coordination of electric and water networks to determine $\bar{\tilde{p}}^R_{i,t}$ in equation (9). As previously mentioned, the PEP method's advantage over other methods (e.g., SO) is that it does not require the assumption of an underlying (joint) probability distribution function of stochastic parameter(s). This is useful in problems like the one considered in which a large volume of historical datasets of the stochastic parameters is available, but it is extremely difficult to get an explicit joint probability distribution function. The data-driven PEP method that solves VRE generation efficient points using historical data at a certain probability level is described as follows.

For the set of historical realizations denoted by $\mathbb{S}$ of the stochastic vector $\tilde{\mathbb{d}} = (\mathbb{d}_1, \ldots, \mathbb{d}_n, \ldots, \mathbb{d}_R)$ for R VRE sites. The $\mathbb{s}^{th}$ sample of the historical realizations of $\tilde{\mathbb{d}}$, is denoted as $\mathbb{d}_{\mathbb{s}} = (\mathbb{d}_{\mathbb{s},1}, \ldots, \mathbb{d}_{\mathbb{s},n}, \ldots, \mathbb{d}_{\mathbb{s},R})$, where $\mathbb{s} \in \mathbb{S}$. The probability of each scenario, $\mathbb{s}$, is denoted as $\mathbb{p}_{\mathbb{s}}$. The MILP in (16)-(20) solves the PEP, as determined in Refs. [40,43].

$$\min_{\mathbb{v}^\beta_1, \ldots, \mathbb{v}^\beta_R} \sum_{n=1}^{R} \mathbb{v}^\beta_n \tag{16}$$

Subject to:

$$\sum_{\mathbb{s} \in \mathbb{S}} \mathbb{p}_{\mathbb{s}} \zeta_{\mathbb{s}} \ge \beta \tag{17}$$

$$\mathbb{v}^\beta_n \ge \mathbb{d}_{\mathbb{s},n} \zeta_{\mathbb{s}}, n = 1, \ldots, R, \mathbb{s} \in \mathbb{S} \tag{18}$$

$$\zeta_{\mathbb{s}} \in \{0,1\}^{|\mathbb{S}|} \tag{19}$$

$$\mathbb{v}^\beta_n \in \mathbb{R}_+, n = 1, \ldots, R \tag{20}$$

The element-wise sum of the PEP vector, $\mathbf{v}^\beta$, guarantees a minimal solution (16). The total probability of a set of samples must at least be equal to the probability level, β, and is satisfied in constraint (17). Equation (18) guarantees each element of the solution ($\mathbb{v}^\beta_n \in \mathbf{v}^\beta$) must be greater than or equal to the corresponding sample in the historical data set ($\mathbb{d}_{\mathbb{s},n} \in \mathbb{d}_{\mathbb{s}}$) of "selected" samples. This is achieved by using binary variable $\zeta_{\mathbb{s}}$ (19), which is one if all constraints $\mathbb{v}^\beta_n \ge \mathbb{p}_{\mathbb{s},n}$, $n = 1, \ldots, R$, are met in the $\mathbb{s}^{th}$ sample, and zero otherwise. The realized solutions must be real, positive values (20). Constraints (17) and (18) require that $\mathbf{v}^\beta$ satisfies the requirement of

a set of scenarios whose aggregate probability is at least equal to the enforced probability level β.

Once the p-efficient point of the VRE generation at probability level β is represented by $\mathbf{v}^{\beta}$, stochastic value $\bar{p}^{R}_{i,t}$ in equation (9) will be replaced by the deterministic value v^{β}_{n}. The PEP model can easily be extended to address uncertainties in electrical load and water demand forecasts. However, we assume these components can be accurately forecasted with a small percent error as opposed to the VRE generation. Therefore, uncertainties associated with electricity and water demands are not considered here.

2.5. DLMP decomposition

We leverage our linearized DLMP model, decomposed in Ref. [40], and extend it to include the flexible demand of the water distribution network. The DLMP components remain the same for this case as the pump demand is not directly related to a marginal increase in electricity demand. Energy, loss, voltage violation, and congestion components are summed to the total real and reactive DLMP ($\Omega^{P}_{i,t}$, $\Omega^{Q}_{i,t}$) as in (21)-(28).

$$\Omega^{P}_{i,t} = \Omega^{E_P}_{i,t} + \Omega^{L_P}_{i,t} + \Omega^{V_P}_{i,t} + \Omega^{C_P}_{i,t} \tag{21}$$

$$\Omega^{Q}_{i,t} = \Omega^{E_Q}_{i,t} + \Omega^{L_Q}_{i,t} + \Omega^{V_Q}_{i,t} + \Omega^{C_Q}_{i,t} \tag{22}$$

$$\Omega^{L_P}_{i,t} = \Omega^{E_P}_{i,t} \sum_{j} \frac{\partial L^{P}_{j,t}}{\partial p_{i,t}} + \Omega^{E_Q}_{i,t} \sum_{j} \frac{\partial L^{Q}_{j,t}}{\partial p_{i,t}} \tag{23}$$

$$\Omega^{L_Q}_{i,t} = \Omega^{E_Q}_{i,t} \sum_{j} \frac{\partial L^{Q}_{j,t}}{\partial q_{i,t}} + \Omega^{E_P}_{i,t} \sum_{j} \frac{\partial L^{P}_{j,t}}{\partial q_{i,t}} \tag{24}$$

$$\Omega^{V_P}_{i,t} = \sum_{i'} (v^{min}_{i',t} - v^{max}_{i',t}) \frac{\partial V_{i',t}}{\partial p_{i,t}} \tag{25}$$

$$\Omega^{V_Q}_{i,t} = \sum_{i'} (v^{min}_{i',t} - v^{max}_{i',t}) \frac{\partial V_{i',t}}{\partial q_{i,t}} \tag{26}$$

$$\Omega^{C_P}_{i,t} = \sum_{j \in u\{i\}} \rho^{1}_{i,t} \frac{\partial S_{j,t}}{\partial p_{i,t}} \tag{27}$$

$$\Omega^{C_Q}_{i,t} = \sum_{j \in u\{i\}} \rho^{2}_{i,t} \frac{\partial S_{j,t}}{\partial q_{i,t}} \tag{28}$$

The shadow prices of (2) and (3) determine the energy component of the DLMP ($\Omega^{E_P}_{i,t}$, $\Omega^{E_Q}_{i,t}$). Loss sensitivities with respect to nodal power injections determine the loss components ($\Omega^{L_P}_{i,t}$, $\Omega^{L_Q}_{i,t}$). Similarly, voltage sensitivities to nodal power injections determine the voltage components ($\Omega^{V_P}_{i,t}$, $\Omega^{V_Q}_{i,t}$). Here, the shadow prices of (14) on all nodes i' that hit a lower or upper voltage limit are captured in $v^{min}_{i',t}$, $v^{max}_{i',t}$. Finally, apparent power flow sensitivities with respect to nodal power injections determine the congestion components ($\Omega^{C_P}_{i,t}$, $\Omega^{C_Q}_{i,t}$). Here, combinations of the four Lagrange multipliers that come from expanding the absolute values in (15) to a linear form are captured in $\rho^{1}_{i,t}$, $\rho^{2}_{i,t}$. The combination of real and reactive power injections is captured in $S_{j,t}$ [40].

3. Water model

The water supply network is modeled as a directed graph $\mathcal{G} = (\mathcal{J}, \mathcal{P})$ with junctions, $\mathcal{J}$, and pipes, $\mathcal{P}$, as nodes and lines of the system. Pipes with pumps ($\mathcal{U}$) and valves ($\mathcal{V}$) are (disjoint, mutually exclusive, independent) subsets of all pipes ($\mathcal{U}$, $\mathcal{V} \in \mathcal{P}$), and reservoirs ($\mathcal{R}$) and tanks ($\mathcal{K}$) are disjoint subsets of junctions ($\mathcal{R}$, $\mathcal{K} \in \mathcal{J}$). Again, we consider time $t \in \mathcal{T}$. Similar to the electricity network, indices i and j' denote the junctions and pipes for the water network. Note, we use index j, without the prime notation, when describing the pipes in the water network in the mathematical model for simplicity, even though the electricity lines and water pipes are independently notated (see Fig. 3.).

Additionally, due to multiple nonconvex constraints, the water model, as is, is NP-hard [18,19]. Therefore, without using solution techniques, exact solutions for the optimal water flow problem are hard to compute, even when the network is small. Here, equations are linearized to reduce the computational burden. Convex relaxation and piecewise linear methods are used. Similar water models can be found in Refs. [18,19].

3.1. Junctions

Water demand, $d_{i,t}$, is considered constant (m^3/h) over the 1-h duration of each time slot. The volumetric flow rate through pipe j is denoted as $f_{j,t}$. Conservation of mass must be followed between two connecting junctions described by their node-line incidence matrix, B (29). Here, $B \in \mathbb{R}^{(\mathcal{J} \times \mathcal{P})}$ is one if pipe j leaves junction i, negative one if pipe j enters junction i, and zero otherwise. This constraint is considered $\forall i \in \mathcal{J}$, $\forall t \in \mathcal{T}$. Each junction i is assigned a minimum and maximum pressure head, $\underline{h}_i$, $\bar{h}_i$, by system operators. For $\forall i \in \mathcal{J}$, $\forall t \in \mathcal{T}$, the head at each junction ($h_{i,t}$) must lie within these two values (30).

$$B \cdot f_{j,t} = d_{i,t} \tag{29}$$

$$\underline{h}_i \le h_{i,t} \le \bar{h}_i \tag{30}$$

3.2. Reservoirs

Reservoirs serve as infinite sources of water to the network, i.e. (29) does not hold, where the junction pressure head (in meters) is zero $\forall i \in \mathcal{R}$, $\forall t \in \mathcal{T}$ as described in (31).

$$h_{i,t} = 0 \tag{31}$$

3.3. Tanks

Tanks are modeled such that the water balance constraint (32) must hold $\forall i \in \mathcal{K}$, $\forall t \in \mathcal{T}$. Denote the volume ($m^3$) in the tank as $u_{i,t}$ and Δt as the time interval between time slots (h). Note, $u_{i,t-1} = u_{i,0}$ for $t = 1$, where $u_{i,0}$ is the initial volume in the tank. Equation (33) restricts the volume of water in the tank to reside between the maximum volume of the tank, $\bar{u}_i$, and the minimum reserve volume, $\underline{u}_i$. The pressure head at the tank, $h_{i,t}$, is defined in (34), and must be greater than zero (35). The bounds for the volumetric flow rate entering (f_{in}) and leaving (f_{out}) the tank are

modeled in (36), where in this instance j represents the upstream and downstream pipes of tank i. Note, $h_{i,t-1} = \frac{u_{i,0}}{A_i}$ for $t = 1$, where A_i is the area of the tank.

$$u_{i,t} = u_{i,t-1} + \Delta t[B \cdot f_{j,t}] \tag{32}$$

$$\underline{u}_i \le u_{i,t} \le \bar{u}_i \tag{33}$$

$$h_{i,t} = h_{i,t-1} + \frac{\Delta t}{A_i}[B \cdot f_{j,t}] \tag{34}$$

$$h_{i,t} \ge 0 \tag{35}$$

$$f_{j,t} \le f_{in}, f_{out} \tag{36}$$

3.4. Pipes without pumps or valves

Head loss across a pipe without a pump or valve ($\breve{h}_{j,t}$) can be modeled using the nonlinear Darcy-Weisbach equation (37) $\forall j \in \mathcal{P}/\mathcal{U} \cup \mathcal{V}$, $\forall t \in \mathcal{T}$. For simplicity, we assume all water pipes are smooth and are modeled using a constant friction factor. Here, $\mathscr{F}_j = \frac{\mu_j l_j}{2 m_j W_j^2 g}$ is a constant related to pipe characteristics such as length (l_j), diameter (m_j), cross-sectional wetted area (W_j), Darcy friction factor (μ_j), and local gravity (g). For volumetric flows in m^3/h, a conversion factor must be included in $\mathscr{F}_j$. Head loss is also calculated as the difference between two junctions surrounding a pipe (38). The flow across a pipe must be positive (39) as we do not consider bidirectional flow in the water model.

$$\breve{h}_{j,t} = \mathscr{F}_j \left(f_{j,t}\right)^2 \tag{37}$$

$$\breve{h}_{j,t} = B^T \cdot h_{i,t} \tag{38}$$

$$f_{j,t} \ge 0 \tag{39}$$

A piecewise linear function further approximates the head loss in (37). A binary variable is used to indicate the section the approximation lies within.

3.5. Variable-speed pumps

A variable speed pump (VSP) moves water through a network [44], by increasing the pressure head across a pipe, $\forall j \in \mathcal{U}$, $\forall t \in \mathcal{T}$. This increase (in meters) is captured in the head gain variable, $\hat{\hat{h}}_{j,t}$, which is modeled by the nonlinear equation (40), where $\omega_{j,t}$ is the actual over nominal pump rotational speed (in rad/s). This value must remain between the minimum and maximum allowable ratios $\underline{\omega}_j$, $\bar{\omega}_j$, if the pump is ON, as indicated by binary variable $\aleph_{j,t}$ (41). Also, note that a_j, b_j, and c_j are the coefficients of the hydraulic characteristics of the pump, where $a_j < 0$; b_j, $c_j > 0$. For simplicity, we assume the efficiency of the pump is constant.

$$\hat{\hat{h}}_{j,t} = a_j (f_{j,t})^2 + b_j f_{j,t} \omega_{j,t} + c_j (\omega_{j,t})^2 \tag{40}$$

$$\underline{\omega}_j \cdot \aleph_{j,t} \le \omega_{j,t} \le \bar{\omega}_j \cdot \aleph_{j,t} \tag{41}$$

Similar to head loss, the head gain between nodes is approximated using a piecewise linear approximation. First, nonlinear equation (40) is modified to eliminate $\omega_{j,t}$ (42), where $b_j^{max} = b_j \cdot \bar{\omega}_j$ and $c_j^{max} = c_j \cdot \bar{\omega}_j^2$. This convex relaxation technique is adopted from Ref. [18] to define an upper bound for the pump head gain. The technique is extended here to enforce a lower bound for the head gain. The right-hand side ($RHS_{j,t}$) of (42) is linearized using a piecewise linear approximation. Similarly, to set a lower bound for the head gain, we use (43), where $b_j^{min} = b_j \cdot \underline{\omega}_j$ and $c_j^{min} = c_j \cdot \underline{\omega}_j^2$. The approximated head gain must be zero or greater than $LHS_{j,t}$. Piecewise linear functions are used to approximate the upper and lower bounds of the head gain, defined in (42) and (43), respectively. The pump rotational speed ratio, $\omega_{j,t}$, can be obtained post-solve.

$$\hat{\hat{h}}_{j,t} \le a_j \left(f_{j,t}\right)^2 + b_j^{max} f_{j,t} + c_j^{max} = RHS_{j,t} \tag{42}$$

$$\hat{\hat{h}}_{j,t} \ge a_j \left(f_{j,t}\right)^2 + b_j^{min} f_{j,t} + c_j^{min} = LHS_{j,t} \cdot \aleph_{j,t} \tag{43}$$

If the pump is ON, the head gain is also captured in the pressure head difference between the two junctions on either side of the pump (44). By use of a binary variable and a large positive constant, M, the pressure head values on either end of the pump are uncoupled if the pump is OFF. The head gain must be a positive value (45), and the water flowing through the pump must be between m and M if the pump is ON (46).

$$-M(1 - \aleph_{j,t}) \le [B^T \cdot h_{i,t}] - \hat{\hat{h}}_{j,t} \le M(1 - \aleph_{j,t}) \tag{44}$$

$$\hat{\hat{h}}_{j,t} \ge 0 \tag{45}$$

$$m \cdot \aleph_{j,t} \le f_{j,t} \le M \cdot \aleph_{j,t} \tag{46}$$

3.6. Pressure reducing valves

Similar to (44) for pumps, but $\forall j \in \mathcal{V}$, $\forall t \in \mathcal{T}$ and where binary variable $\mathbb{y}_{j,t}$ indicates valve ON/OFF state, the head loss, $\hat{\hat{h}}_{j,t}$, is modeled as the difference between the junctions on either end of the valve if the valve is ON (physically meaning open) (47). If the valve is OFF (physically meaning closed), the pressure heads at either end are uncoupled. If the valve is ON, the head loss must be greater than zero (48), and the flow through the valve must be positive (49).

$$-M(1 - \mathbb{y}_{j,t}) \le [B^T \cdot h_{i,t}] - \breve{h}_{j,t} \le M(1 - \mathbb{y}_{j,t}) \tag{47}$$

$$\breve{h}_{j,t} \ge 0 \tag{48}$$

$$m \cdot \mathbb{y}_{j,t} \le f_{j,t} \le M \cdot \mathbb{y}_{j,t} \tag{49}$$

When the valve is ON, i.e., open, the valve acts like a pipe. Therefore, pressure head loss across the pipe is also modeled using the approximation in (37), $\forall j \in \mathcal{V}$, $\forall t \in \mathcal{T}$.

3.7. Power consumption of pumps

The real power consumed by the pump, denoted by variable $p_{j,t}^{D,U}$, $\forall j \in \mathcal{U}$, $\forall t \in \mathcal{T}$ is modeled in nonlinear equation (50), where ρ_w, g, and η_j denote the water density, acceleration due to gravity,

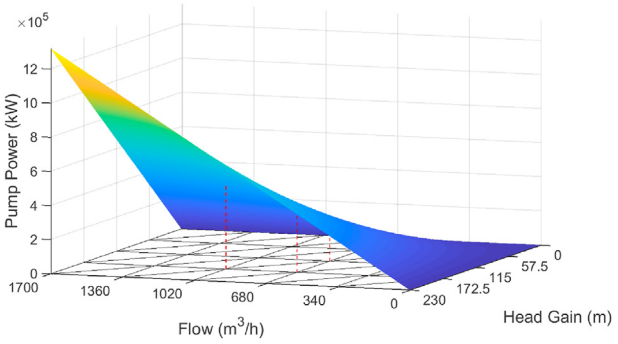

Fig. 2. Pump power linear approximation using the 2D piecewise linearization method.

and the efficiency of the pump, respectively. For our purposes, we assume the reactive power of the pump, $q_{j,t}^{D,U}$, is κ^W of the real power.

$$p_{j,t}^{D,U} = \frac{\rho_w g}{\eta_j} \hat{h}_{j,t} f_{j,t} \tag{50}$$

The power consumed by the pump is approximated using a 2D piecewise linear method, namely convex combination triangulation, $\forall j \in \mathcal{U}$, $\forall t \in \mathcal{T}$ as in (51). Variables $\mathscr{A}_{tri}$, $\mathscr{B}_{tri}$, and $\mathscr{C}_{tri}$ are determined by using the results of (50) evaluated at the boundaries, $f_{tri,j,t}$ and $\hat{\hat{h}}_{tri,j,t}$, of each nonoverlapping triangle. A binary indicator, $\mathbb{T}_{tri,j,t}$, is used to determine which triangle approximates the pump power. Convex combination theory is used to locate the flow and head gain values into a single triangle. This technique is believed to be sufficient as the resulting graph of the pump power has no drastic curves and allows for a straightforward mapping of the linear convex polytopes, as shown in the linear approximation mapping in Fig. 2. The red dashed lines indicate the 2D triangular approximation bounds that intercept the actual, nonlinear pump power graph within a specific segment of head gain and volumetric flow rate values.

$$p_{j,t}^{D,U} = \sum_{tri} \mathscr{A}_{tri} \cdot f_{tri,j,t} + \mathscr{B}_{tri} \cdot \hat{\hat{h}}_{tri,j,t} + \mathscr{C}_{tri} \cdot \mathbb{T}_{tri,j,t} \tag{51}$$

The linear water flow problem now consists of constraints (29)-(36), (38)-(39), (42)-(49), (51), and the additional constraints associated with the linear approximation of head gain, head loss, and pump power. Note, the accuracy of the water model will improve with more piecewise linearization segments or triangles at the cost of lower computational efficiency. The longer solving times that arise from a higher number of segments/triangles can be managed in the day-ahead scheduling timeframe.

3.8. Pump cost calculation

The pump electricity cost calculation (52), captured by C_w, is found by multiplying the real and reactive power consumed by the pumps applied to connected node i ($p_{i,t}^{D,U}$, $q_{i,t}^{D,U}$), and the total real and reactive DLMP ($\Omega_{i,t}^{P}$, $\Omega_{i,t}^{Q}$) at the node the pump's load is applied.

$$C_w = \sum_{i,t} p_{i,t}^{D,U} \cdot \Omega_{i,t}^{P} + \sum_{i,t} q_{i,t}^{D,U} \cdot \Omega_{i,t}^{Q} \tag{52}$$

3.9. Merged water and power flow problem

Finally, the merged optimal water and power flow problem is considered as $\mathbf{P_1}$. In this model, we consider the water network as a demand response system. The water network is not optimized for the least cost of pumping, but all water constraints must be met. Here, $p_{i,t}^{D}$ in (4) is a summation of the non-pump electrical demand $p_{i,t}^{D,N}$ and the calculated pump demand associated with its respective node i, $p_{i,t}^{D,U}$. A similar coupling can be made for reactive power demand. We define the coupled optimal water and power flow problem, $\mathbf{P_1}$, as:

$\mathbf{P_1}$: min (1) subject to: (2)–(15), (29)–(36), (38)–(39), (42)–(49), (51), and linear approximation constraints.

We acknowledge an MILP model with piecewise linear approximations requires more time to solve than other methods, such as a second-order cone (SOC) model, as verified in Ref. [24]. That said, the MILP model has an advantage over the SOC model presented in Ref. [18] when used with nodal DLMPs. The objective function of the SOC model in Ref. [18] must minimize energy losses in the water network. Therefore, the energy consumed by the pumps is not minimized using dynamic electricity prices, such as DLMPs, but is calculated post-solve. Also, the pump power consumption is only modeled post-solve and, thus, is not suitable for

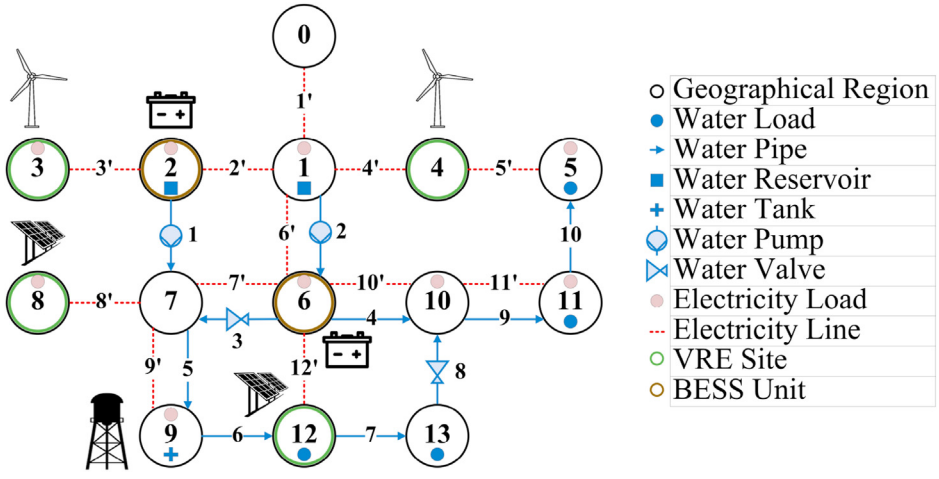

Fig. 3. Integrated IEEE 13-node electricity and 10-node water distribution networks.

our proposed merged model without modification. Therefore, we use the MILP model in this work. Furthermore, we assume the DSO is equipped with the computational capability to handle computationally intensive problems within a reasonable amount of time. This assumption holds even if a large number of historical VRE samples are employed by the PEP method. We believe this is a valid assumption based on the quality/number of commercially available MILP solvers today. However, if issues arise from computational complexities, sample reduction, bundling, or other state-of-the-art techniques can ease the solver's burden.

4. Case study

To validate our proposed model, we consider a modified IEEE 13-bus distribution system connected to a 10-bus water distribution network, as Fig. 3 displays. This network mimics a realistic small-town or urban electrical distribution network, serving a peak power demand of approximately 1.3 MW with a feeder length of 1.65 miles. VRE generation units are at Nodes 3, 4, 8, and 12, and BESS units are at Nodes 2 and 6. The energy demands for the pumps in the water network are included in the electrical demand for Nodes 1 and 2. A yearlong sample of hourly wind and PV generation at two sites was obtained from the Western Wind and Solar Integration Study (WWSIS) historical data sets [46]. These data were used to obtain the daily VRE generation time series using the PEP method and then scaled to match our system. Identical sets of data were used for VRE units located in close proximity to one another.

Of similar topology to Refs. [19,47], the water supply network consists of two reservoirs, two VSPs, one tank, and two valves. We assume the elevation of all junctions in the water network to be zero (m). The minimum head at demand nodes is $\underline{h}_i = 5$ (m). The tank area is $A_9 = 490.87$ (m^2), and the maximum volume of the tank is $\bar{u}_9 = 14{,}726.1$ (m^3), i.e., the tank is 30 m tall. The minimum allowable volume, $\underline{u}_9$, is 10% of the maximum volume, and the initial volume in the tank is $u_{9,0} = 9100$ (m^3), which is approximately 18.5 (m) of water. The maximum allowable flow in and out of the tank is 1100 (m^3/h). The pipe and activated valve parameters are modified versions of the network in Ref. [47], and we consider the Darcy friction factor of each pipe used in Equation (37) to be $\mu_j = 0.014$. From Ref. [44], the parameters of the VSPs are $a_j = -1.0941 \times 10^{-4}$, $b_j = 5.1516 \times 10^{-2}$, $c_j = 223.32$, $\bar{\omega} = 1$, and $\underline{\omega} = 0.2$. The pump efficiency is assumed to be constant at all speeds, $\eta_j = 80.75\%$. The total water demand is depicted in Fig. 5. We consider the power and water flows to be in steady-state within the 1-h timeslots. This time resolution is sufficient for the day-ahead energy trading market. Further, our model could equivalently serve in the real time market with 5- to 15-min time intervals. GAMS/CPLEX 28.1.0 [45] is used to solve the proposed MILP, $\mathbf{P_1}$. We create the following scenarios:

Scenario 1: PEP Probability Level – Comparison of VRE output at $\beta = 25\%$, $\beta = 50\%$, and $\beta = 75\%$. Note, we assume probabilities and probability levels are known to the DSO a priori.
Scenario 2: High VRE – Coupled water and electricity networks ($\mathbf{P_1}$) with high VRE penetration are compared with and without a water tank.

4.1. Impact of PEP probability level on VRE output

Changing the PEP probability level, as in Scenario 1, has a considerable impact on the expected VRE generation, as shown in Fig. 4. Hourly wind and solar generation data are obtained from WWSIS and used to find the probability efficient point at different probability levels using the PEP method. The higher the probability level (β), the higher the expected wind and solar generation. Wind generation outputs face more substantial differences between probability levels because the data has a broader range of historical samples than the relatively narrow band of PV data. The output at a given PEP is applied to each VRE site, respective of the generation type. We assume the same result for different sites of the same technology as the generation units are considered to be in close proximity to each other and therefore see the same resource.

4.2. Impact of tank as storage device

Considering the parameters of Scenario 2, we investigate the impact of the tank as an energy storage device. Instead of curtailing wind and solar energy, the water network utilizes pumps to store water in tanks to use when non-pump electricity demands are high. Table 2 outlines the cost and demand comparison of a system with and without a tank at probability level $\beta = 75\%$. The costs for each network are very similar in each case, yet the pump demand is increased for the case with a tank. The negative electricity cost is due to the selling of excess VRE to the grid in all timeslots. Though the difference in the VRE utilization factors (the amount of dispatched VRE over the total generated) is small, the case with the tank recovers 124.3 kWh of VRE that is otherwise curtailed in the case without a tank.

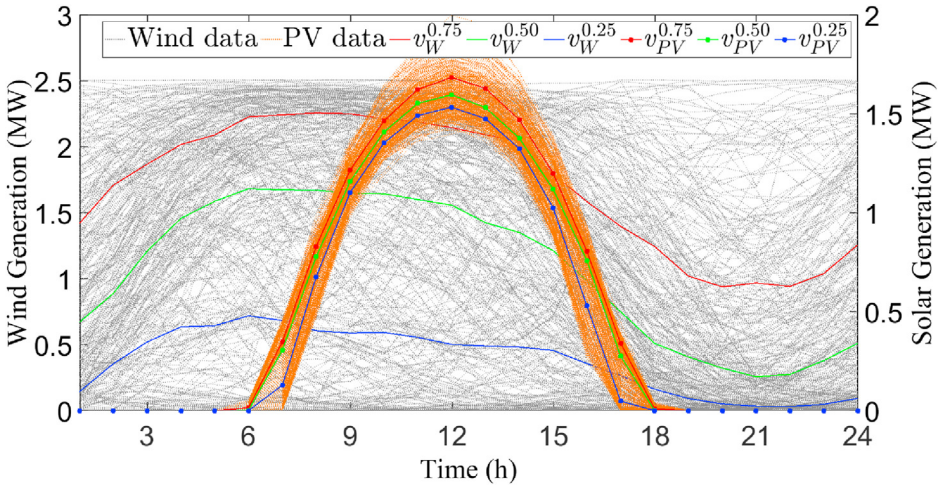

Fig. 4. Historical wind (W) and PV data and the PEP result at 25%, 50%, and 75% probability levels.

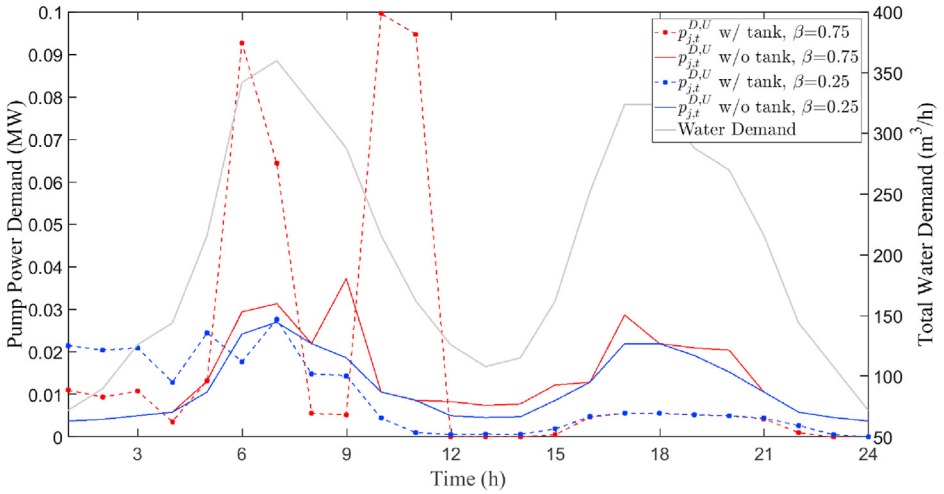

Fig. 5. Summed pump power ($\sum_j p_{j,t}^{D,U}$, where $j \in \mathcal{U}$) schedule versus water demand at probability levels 25% and 75%.

Table 2
Scenario 2 daily results at $\beta = 75\%$ (*Calculated post-solve using (52)).

	Tank	No Tank
C_e	-$1954.59	-$1953.15
C_w	$5.18*	$5.85*
Pump Energy	442.7 kWh	337.3 kWh
Energy Consumed	23.19 MWh	23.08 MWh
VRE Recovery	124.3 kWh	–
VRE Utilization	93.4%	93.2%

The differences in pump schedules for cases with and without a tank in the water network at different PEP probability levels are depicted in Fig. 5. For the case with a tank, the pump schedule shifts the peak power consumption so that it no longer aligns with the peaks and valleys of the water demand, as it must for the case without a tank. In the cases with probability level $\beta = 25\%$, the available VRE is lower, and therefore, the difference in the pump schedule with and without a tank is minimal compared to $\beta = 75\%$. The case with a tank and $\beta = 75\%$, in general, sees more substantial pump power demands in the first half of the day. The additional power supplied to the pumps is an attempt to better utilize the high VRE generation by storing water in the tank during the daytime and enables the water network to serve as a demand response mechanism. Note, in a standalone water network without considering VREs, one can expect the pump power demand to decrease with the addition of a water tank in the network. However, this is not the case for this work as the water tank acts as an electricity storage device and consumes excess VRE power; thus, pump power demand increases with the addition of a water tank in the proposed merged water and energy problem. This result demonstrates the necessity of a coordinated operation of water and electricity distribution networks when VRE generation is in place.

4.3. Impact of PEP probability level

The water storage in the tank at different probability levels is graphically represented in Fig. 6. As expected, the VRE curtailment is higher in the cases without a tank. Note, the cases with a tank at probability levels $\beta = 75\%$ and $\beta = 50\%$ slightly reduce the VRE curtailment by storing water in the tank. The case with probability level $\beta = 25\%$ does not curtail VRE generation as the VRE output is entirely used by the system both with and without a tank. The reduction in VRE curtailment is limited by the maximum inflow constraint into the tank and potential voltage violations and line congestion in the electricity network from moving large amounts of

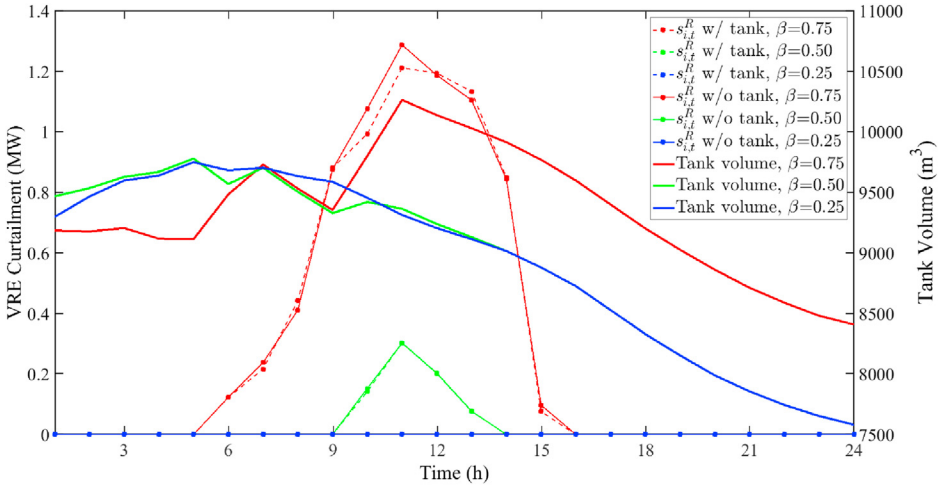

Fig. 6. VRE curtailment summed over the generation locations ($\sum_i s_{i,t}^R$, where $i \in G$) and tank volume at 25%, 50%, and 75% probability levels for cases with and without a tank.

Table 3
Scenario 2 Results with Changing β

Probability Level	VRE Recovery
$\beta = 0.75$	124.3 kWh
$\beta = 0.50$	7.9 kWh
$\beta = 0.25$	0 kWh

power to the nodes with flexible water pumps. Also, the comparatively smaller power demands of the pumps limit the impact of reducing VRE curtailment. The tank fills to aid in the electricity network's health by reducing line congestion and voltage violations. The final tank volume for $\beta = 75\%$ is greater than the other two probability levels because the tank acts as a battery and stores a greater amount of excess VRE in this case. Table 3 outlines the amount of VRE generation recovered in the case with a tank versus the case without a tank at different probability levels. The water tank allows less VRE generation to be curtailed in a case of excess VRE generation. As the probability level decreases, and subsequently, the VRE generation, the VRE recovery decreases because the system is able to use more of the VRE generation. Again, the system completely uses all VRE generation at probability level $\beta = 25\%$, so there is no excess VRE generation to store as potential energy in the water tank in this case.

4.4. Impact of tank on DLMP

Considering the constraints of Scenario 2 and the PEP probability level at $\beta = 75\%$, we observe the impact of the tank on the real power DLMP, as shown in Fig. 7. Negative real power components indicate some part of the system, respective of each component, would benefit from more real power consumption at that node. However, the total nodal DLMP (red line with asterisks) may still be positive overall. Also, losses are unavoidable and, therefore, loss DLMP components occur in every timeslot.

Fig. 7 graphically depicts the differences in the component-wise DLMP for the case with and without a tank on Node 1. Due to the selling of excess VRE generation to the grid, congestion occurs on Lines 1' and 3' in many timeslots. In the case with the tank, the congestion is completely removed from Line 1' in Timeslots 10 and 11. With the freed line capacity in the case with a tank, the VRE units sell power until the point that the maximum voltage constraint is met on Nodes 3, 8, and 12, and larger voltage DLMP components replace the congestion DLMP components in Timeslots 10 and 11. Note, the voltage DLMP components in Timeslots 10 and 11 in the case without a tank are relatively small and are not visible in the figure. The allowance of curtailing VRE generation is put in place to avoid voltage violations and congestion.

Adding the tank produces small changes in the VRE curtailment reduction and DLMPs. This impact could be amplified with additional or larger tanks in the water network and longer simulated timeframes. In a potential future case with large amounts of VRE penetration in the distribution network, storage devices will be necessary to reduce VRE generation curtailments. Storing water in existing water tanks may be a low-cost option that can positively impact, even if in a small way, the electricity network by reducing voltage violations and line congestion. Utilizing water tanks as storage devices may not altogether remove the VRE overgeneration, and the system may see more benefits from a diverse storage profile. That said, the cooperation of the water and electricity networks can adequately serve as demand response and a storage technology to improve the health of the electric distribution network while still meeting water demands.

4.5. Impact of failures

To investigate the impact of failures in the proposed model, we test the system behavior when a component in the coupled model fails. A failed component could be caused by damage to the component in an extreme event, such as a weather-related occurrence or even a malicious, targeted attack on the system. We consider a case where the valve on Pipe 8 (see Fig. 3) faces a failure, i.e., Valve 8 is forced closed and does not allow water flow over the pipe. Fig. 8 shows the result of this study. Fig. 8(a) compares the VRE curtailment and tank volume over the scheduling period for normal and failed operating conditions. Fig. 8(b) depicts the resulting DLMP of Node 1 after the failure of Valve 8. Congestion occurs on Line 1' in Timeslots 9, 10, and 11.

Interestingly, the DLMP looks very similar to the DLMP in Fig. 7(b). There is a larger congestion DLMP component in Timeslot

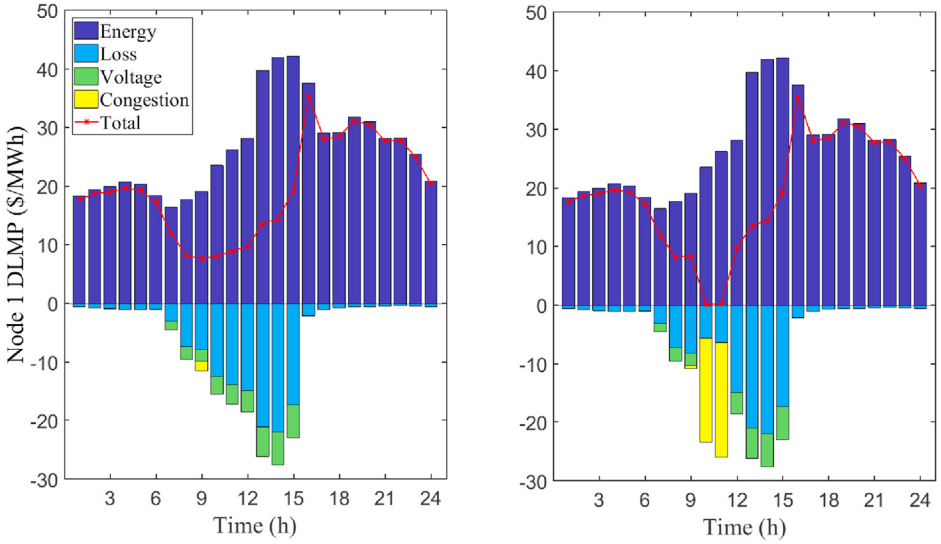

(a) DLMP with tank (b) DLMP without tank

Fig. 7. Node 1 component-wise DLMP at a 75% probability level for cases with and without a tank.

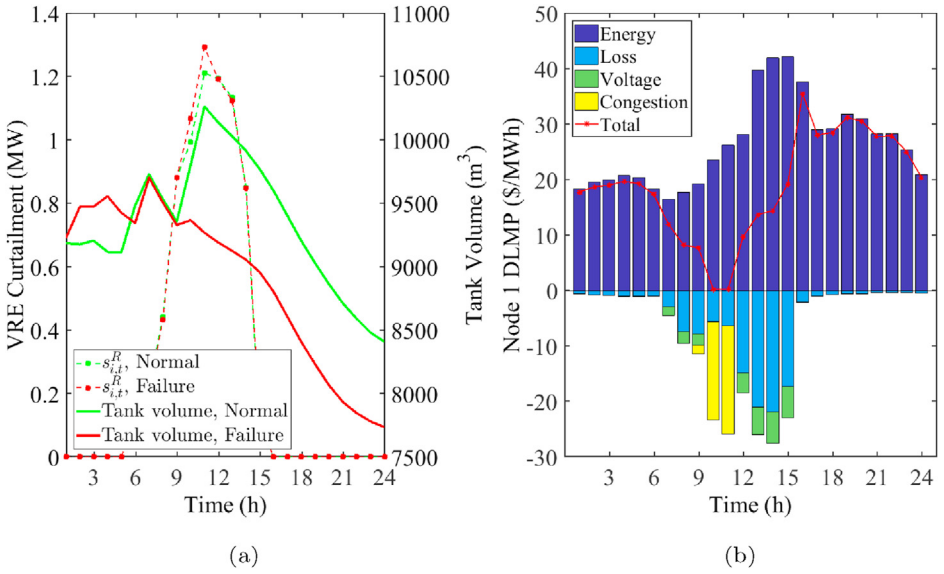

Fig. 8. VRE curtailment and tank volume for normal operating conditions versus system behavior with Valve 8 failure (a); resulting DLMP of Node 1 with Valve 8 failure (b). Both subplots consider $\beta = 75\%$ and tank inclusion in the model.

9 in the system with Valve 8 failure than in the case without a tank. This congestion is caused by the desire to sell excess VRE generation to the grid at LMP (of the substation node) rather than fill the tank to use for water demand at later hours in the day. In the system with a failed Valve 8, the tank can only serve the water demands at Junctions 12 and 13. Note, in Timeslots 11–24, the water tank completely fulfills the water demands at Junctions 12 and 13, i.e., Pump 1 is not operating and Valve 3 is open.

Furthermore, the tank can no longer reach the water demands at Junctions 5, 10, and 11, whose additional water demands were a great motivator in filling the tank in a case with excess VRE. This observation is further illustrated in Fig. 8(a) as we do not see the tank store as much water as it would under normal operating conditions. With a failure at Valve 8, Pump 2 runs in every timeslot to meet the water demands of Junctions 10, 11, and 5. Even though Pump 2 is on in all timeslots, the total daily energy consumed by both pumps is still less than the fully operational case with a tank. Therefore, the system with Valve 8 failure also sees slightly more VRE curtailment than its fully operational counterpart. This study shows failures in the water network can impact the DLMP and overall health of the electricity distribution network.

5. Conclusion

Numerical results show the advantages of combining these two networks and utilizing water pumps and tanks as jointly flexible loads. For the first time, the following observations can be made.

- The water network can positively impact the DLMP by minimally reducing voltage violation and congestion penalties when VRE penetration is high. By optimally scheduling the water tank, the congestion on certain electricity distribution lines can be eliminated. In many cases, the water tank storage prevents line congestion and binding nodal voltage constraints. As a result, it can ease the operational challenges in the electricity distribution network.
- In a high VRE scenario, the tank aids in lowering the curtailment of VREs by filling over time to absorb excess VRE generation in the system, though typically by a small amount due to relatively small pump demands and limited tank capacity.
- The use of the water tank allows the peak pump demand to shift away from the non-pump peak electricity demand, reducing the total peak electricity demand. From the perspective of the electricity DSO, an advantage of combining the two networks comes in the form of congestion relief in the electricity distribution network.
- When combined with VRE generation, the coordinated water and electricity network offers a unique storage solution of excess VRE generation through the use of the water tank. Similar to a battery, the tank will store water to use later when there is more VRE generation in the system than there is demand.
- The data-driven PEP method with different probability levels can impact the coordinated operation of the water and electricity networks and the VRE curtailment, which provides a means to manage the VRE uncertainty.
- Failed components in one network are capable of changing system behavior in the other network.

In this paper, a novel coordinated water and energy model was formulated and validated on a coupled IEEE 13-node electrical distribution network and 10-node water network. The proposed method can impact policies regarding interdependent water and energy networks, especially those seeing significant increases in VRE generation. Under the consideration of VRE uncertainty, the impact of the coupling of the water and electricity networks on the DLMP was shown for the first time. Further, it was shown how the coupling of the water and electricity distribution networks could supplement future distribution markets that consider DLMP. Note, the cost of storing energy in water tanks is not considered in this work. Interesting further work includes quantifying a financial incentive beyond the benefits from DLMP that can be allocated to water utilities for providing demand response services to the electricity DSO. The financial incentive should include compensation for accelerated aging of the pumps, increased energy prices, etc. This financial incentive can be easily added to the proposed model. This cooperation could help water utilities reduce operational costs.

The proposed model and method can offer utilities a new tool in managing the coordinated operation of water and electricity distribution networks under uncertain VRE generation. With the recent call for more energy-efficient systems, the approach

provided in this work can serve as an energy-saving solution to water and electric utility operators. As longer solving times in day-ahead optimization problems are not a pressing issue, this model should scale with ease. If the larger system is unable to solve in a reasonable time, authors in Ref. [48] have proposed a clustering technique to combat this issue. While we consider energy storage and demand response through drinking water storage tanks in this work, this study can be extended to various types of flexible loads that can act as an energy storage medium, each with its own set of benefits, challenges, and limitations to consider. For example, staying within the subject of the water-energy nexus, water purification through reverse osmosis could serve as a demand-responsive load. Our future work includes extending the model to a three-phase unbalanced electrical distribution system and optimizing the water network based on electricity price signals through a bi-level optimization problem using DLMPs. Cyberattacks and their impact on the interdependent networks will also be considered.

Declaration of competing interest

The authors declare that they have no known competing financial interests or personal relationships that could have appeared to influence the work reported in this paper.

References

[1] C.A. Dieter, et al., Estimated use of water in the United States in 2015: U.S, Geol. Surv. Circular 1441 (2018).
[2] The Water-Energy Nexus: Challenges and Opportunities, U.S. Department of Energy, Washington, DC, USA, Jun. 2014, p. 262. DOE/EPSA-0002.
[3] Food and Agriculture Organization of the United Nations, The State of the World's Land and Water Resources for Food and Agriculture: Managing Systems at Risk, first ed., Routledge, 2013.
[4] National Water Program 2012 Strategy: Response to Climate Change, United States Environmental Protection Agency, Dec. 2012, p. 132.
[5] S.O. Muhanji, C. Barrows, J. Macknick, A.M. Farid, An enterprise control assessment case study of the energy–water nexus for the ISO new England system, Renew. Sustain. Energy Rev. 141 (May 2021) 110766.
[6] J. Lv, Y.P. Li, G.H. Huang, C. Suo, H. Mei, Y. Li, Quantifying the impact of water availability on China's energy system under uncertainties: a perceptive of energy-water nexus, Renew. Sustain. Energy Rev. 134 (Dec. 2020) 110321.
[7] W. Hickman, A. Muzhikyan, A.M. Farid, The synergistic role of renewable energy integration into the unit commitment of the energy water nexus, Renew. Energy 108 (Aug. 2017) 220–229.
[8] E. Ahmadi, B. McLellan, T. Tezuka, The economic synergies of modelling the renewable energy-water nexus towards sustainability, Renew. Energy 162 (Dec. 2020) 1347–1366.
[9] P.H. Gleick, Water and energy, Annu. Rev. Energy Environ. 19 (1) (1994) 267–299.
[10] S.W.D. Turner, M. Hejazi, K. Calvin, P. Kyle, S. Kim, A pathway of global food supply adaptation in a world with increasingly constrained groundwater, Sci. Total Environ. 673 (Jul. 2019) 165–176.
[11] Water and Wastewater Annual Price Escalation Rates for Selected Cities across the United States, DOE Office of Energy Efficiency and Renewable Energy, DOE/EE-1670, Sep. 2017, p. 1413878.
[12] Flexible Resources Help Renewables Fast Facts, California ISO, Folsom, CA, USA, 2016.
[13] T. Edmunds, et al., The Value of Energy Storage and Demand Response for Renewable Integration in California, California Energy Commission, Feb. 2017, p. 241.
[14] P. Denholm, Y.H. Wan, M. Hummon, M. Mehos, "Analysis of Concentrating Solar Power with Thermal Energy Storage in a California 33% Renewable Scenario," Nat. Renewable Energy Lab., Golden, CO, USA, Tech. Rep., NREL/TP-6A20-58186, 1072790, Mar. 2013.
[15] A. Botterud, T. Levin, V. Koritarov, "Pumped Storage Hydropower: Benefits for Grid Reliability and Integration of Variable Renewable Energy," Argonne Nat. Lab. Report ANL/DIS-14/10, Argonne, IL, USA, Aug. 2014.
[16] E. Ela, "Role of Pumped Storage Hydro Resources in Electricity Markets and System Operation: Preprint," NREL Conference Paper, May 2013, p. 12.
[17] K. Mongird, et al., "Energy Storage Technology and Cost Characterization Report," PNNL-28866, vol. 1573487, Jul. 2019.
[18] D. Fooladivanda, J.A. Taylor, Energy-optimal pump scheduling and water flow, IEEE Trans. Control Netw. Syst. 5 (3) (Sep. 2018) 1016–1026.
[19] A.S. Zamzam, E. Dall'Anese, C. Zhao, J.A. Taylor, N. Sidiropoulos, Optimal water-power flow problem: formulation and distributed optimal solution, IEEE Trans. Control Netw. Syst. 6 (1) (Jan. 2018) 37–47.
[20] K. Oikonomou, M. Parvania, R. Khatami, Optimal demand response scheduling for water distribution systems, IEEE Trans. Ind. Inform. 14 (11) (Nov. 2018) 5112–5122.
[21] K. Oikonomou, M. Parvania, Optimal coordination of water distribution energy flexibility with power systems operation, IEEE Trans. Smart Grid 14 (11) (Apr. 2018) 1101–1110.
[22] K. Oikonomou, M. Parvania, Optimal coordinated operation of interdependent power and water distribution systems, IEEE Trans. Smart Grid 11 (6) (Nov. 2020) 4784–4794.
[23] F. Moazeni, J. Khazaei, Optimal operation of water-energy microgrids; A mixed integer linear programming formulation, J. Clean. Prod. 275 (Dec. 2020) 122776.
[24] C. Wang, N. Gao, J. Wang, N. Jia, T. Bi, K. Martin, Robust operation of a water-energy nexus: a multi-energy perspective, IEEE Trans. Sustain. Energy 11 (4) (Oct. 2020) 2698–2712.
[25] M. Shahidehpour, H. Wu, "Hourly Demand Response as an Alternative to Flexible Ramping of Thermal Units in Stochastic Operation of Electric Power Systems with Non-dispatchable Energy Sources," in *Handbook Of Clean Energy Systems*, Jun. 2015.
[26] H. Wu, M. Shahidehpour, Z. Li, W. Tian, Chance-constrained day-ahead scheduling in stochastic power system operation, IEEE Trans. Power Syst. 29 (4) (Jul. 2014) 1583–1591.
[27] C. Dai, L. Wu, H. Wu, A multi-band uncertainty set based robust SCUC with spatial and temporal budget constraints, IEEE Trans. Power Syst. 31 (6) (Nov. 2016) 4988–5000.
[28] C. Wan, Z. Xu, P. Pinson, Z.Y. Dong, K.P. Wong, Optimal prediction intervals of wind power generation, IEEE Trans. Power Syst. 29 (3) (May 2014) 1166–1174.
[29] H. Wu, et al., Stochastic multi-timescale power system operations with variable wind generation, IEEE Trans. Power Syst. 32 (5) (Sep. 2017) 3325–3337.
[30] A. Zakaria, F.B. Ismail, M.H. Lipu, M.A. Hannan, Uncertainty models for stochastic optimization in renewable energy applications, Renew. Energy 145 (Jan. 2020) 1543–1571.
[31] A. Prékopa, Dual method for the solution of a one-stage stochastic programming problem with random RHS obeying a discrete probability distribution, Z. Oper. Res. 34 (6) (Nov. 1990) 441–461.
[32] H. Masri, F.B. Abdelaziz, I. Meftahi, "A Multiple Objective Stochastic Portfolio Selection Program with Partial Information on Probability Distribution," in 2010 Second International Conference on Computer and Network Technology, Apr. 2010, pp. 536–539.
[33] M.R. Murr, A. Prékopa, Solution of a product substitution problem using stochastic programming, in: S.P. Uryasev (Ed.), In Probabilistic Constrained Optimization: Methodology and Applications, Springer US, Boston, MA, 2000, pp. 252–271.
[34] A. Yazici, K. Ozbay, Evacuation network modeling via dynamic traffic assignment with probabilistic demand and capacity constraints, Transport. Res. Rec. 2196 (1) (Jan. 2010) 11–20.
[35] C. Zhao, R. Jiang, Distributionally robust contingency-constrained unit commitment, IEEE Trans. Power Syst. 33 (1) (Jan. 2018) 94–102.
[36] M.J. Reno, R.J. Broderick, Statistical Analysis of Feeder and Locational PV Hosting Capacity for 216 Feeders, IEEE Power and Energy Society General Meeting (PESGM), Boston, MA, USA, Jul. 2016, pp. 1–5.
[37] E. Ela, et al., Future electricity markets: designing for massive amounts of zero-variable-cost renewable resources, IEEE Power Energy Mag. 17 (6) (Nov. 2019) 58–66.
[38] L. Edmonds, M.N. Faqiry, H. Wu, A. Palani, Three-Phase Distribution Locational Marginal Pricing to Manage Unbalanced Variable Renewable Energy, Jan. 2020.
[39] M.N. Faqiry, L. Edmonds, H. Zhang, A. Khodaei, H. Wu, Transactive-market-based operation of distributed electrical energy storage with grid constraints, Energies 10 (11) (Nov. 2017) 1891.
[40] M.N. Faqiry, L. Edmonds, H. Wu, A. Pahwa, Distribution locational marginal price-based transactive day-ahead market with variable renewable generation, Appl. Energy 259 (Feb. 2020) 114103.
[41] H. Yuan, F. Li, Y. Wei, J. Zhu, Novel linearized power flow and linearized OPF models for active distribution networks with application in distribution LMP, IEEE Trans. Smart Grid 9 (1) (Jan. 2018) 438–448.
[42] J.A. Taylor, Convex Optimization of Power Systems, Cambridge University Press, 2015.
[43] M. Lejeune, N. Noyan, Mathematical programming approaches for generating p-efficient points, Eur. J. Oper. Res. 207 (22) (Dec. 2010) 590–600.
[44] B. Ulanicki, J. Kahler, B. Coulbeck, Modeling the efficiency and power characteristics of a pump group, J. Water Resour. Plann. Manag. 134 (1) (Jan. 2008) 88–93.
[45] GAMS Development Corporation, General Algebraic Modeling System (GAMS) Release 28.1.0, GAMS Development Corporation, Washington, DC, USA, 2019.
[46] D. Lew, et al., "The Western Wind and Solar Integration Study Phase 2," Nat. Renewable Energy Lab., Golden, CO, USA, Tech. Rep., NREL/TP–5500-55588, vol. 1220243, Sep. 2013.
[47] D. Cohen, U. Shamir, G. Sinai, Optimal operation of multi-quality water supply systems-II: the Q-H model, Eng. Optim. 32 (6) (Jan. 2000) 687–719.
[48] W. Wang, R. Jing, Y. Zhao, C. Zhang, X. Wang, A load-complementarity combined flexible clustering approach for large-scale urban energy-water nexus optimization, Appl. Energy 270 (Jul. 2020) 115163.